GASTRO ENTEROLOGIA BELLUNO

Con il patrocinio di

PROGRESSI E NUOVE FRONTIERE IN
GASTROENTEROLOGIA ED ENDOSCOPIA DIGESTIVA

BELLUNO
15-16 GIUGNO 2023

Ruolo della Intelligenza Artificiale in epatologia

Domenico ALVARO, MD

Sapienza, University of Rome, Italy

Con il patrocinio di

GASTRO ENTEROLOGIA BELLUNO

aigo · S.I.E.D. · SIGE · fismad

PROGRESSI E NUO
GASTROE

MEDIATECH:Martedì, 30/5/2023

"L'intelligenza artificiale come una guerra nucleare. Umanità a rischio"

L'allarme clamoroso di 350 esperti tra cui l'ad di OpenAI, Sam Altman, e il fisico italiano Roberto Battiston

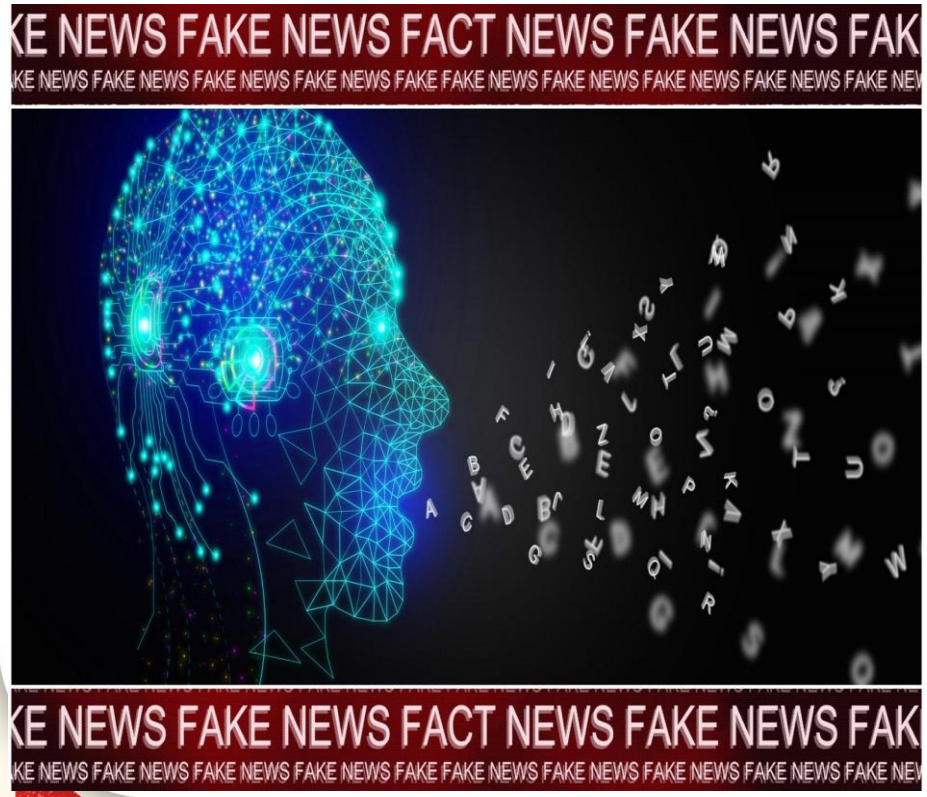

ChatGPT, Bard e ErnieBot: perché chiedere all'intelligenza artificiale non è sempre intelligente

Cosa sono e come funzionano i chatbot basati sull'intelligenza artificiale e perché i limiti sono ancora molti

Ethical code related to Artificial Intelligence Tools

This lecture is the result of

Arificial Intelligence
OR
My Natural Deficiency

The NEW ENGLAND JOURNAL of MEDICINE

REVIEW ARTICLE

Jeffrey M. Drazen, M.D., *Editor;*
Isaac S. Kohane, M.D., Ph.D., and Tze-Yun Leong, Ph.D., *Guest Editors*

AI IN MEDICINE

Artificial Intelligence and Machine Learning in Clinical Medicine, 2023

Charlotte J. Haug, M.D., Ph.D., and Jeffrey M. Drazen, M.D.

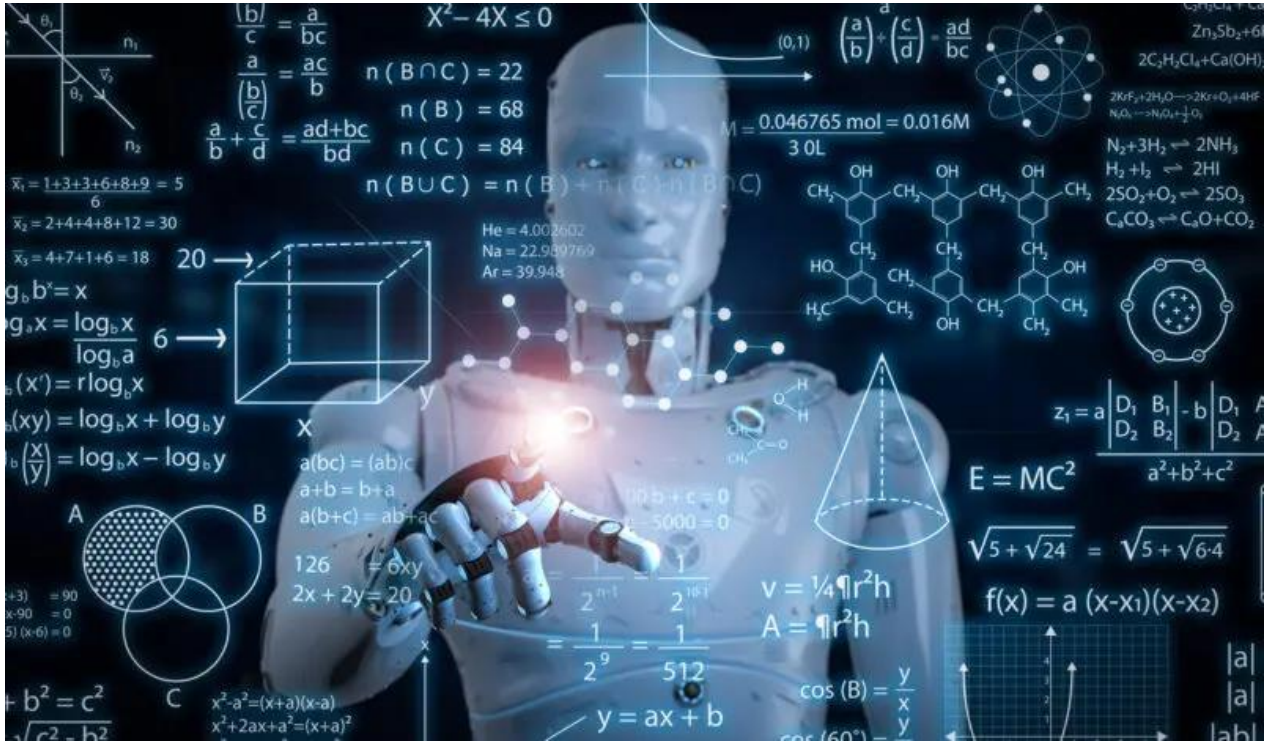

B Advances in Speed

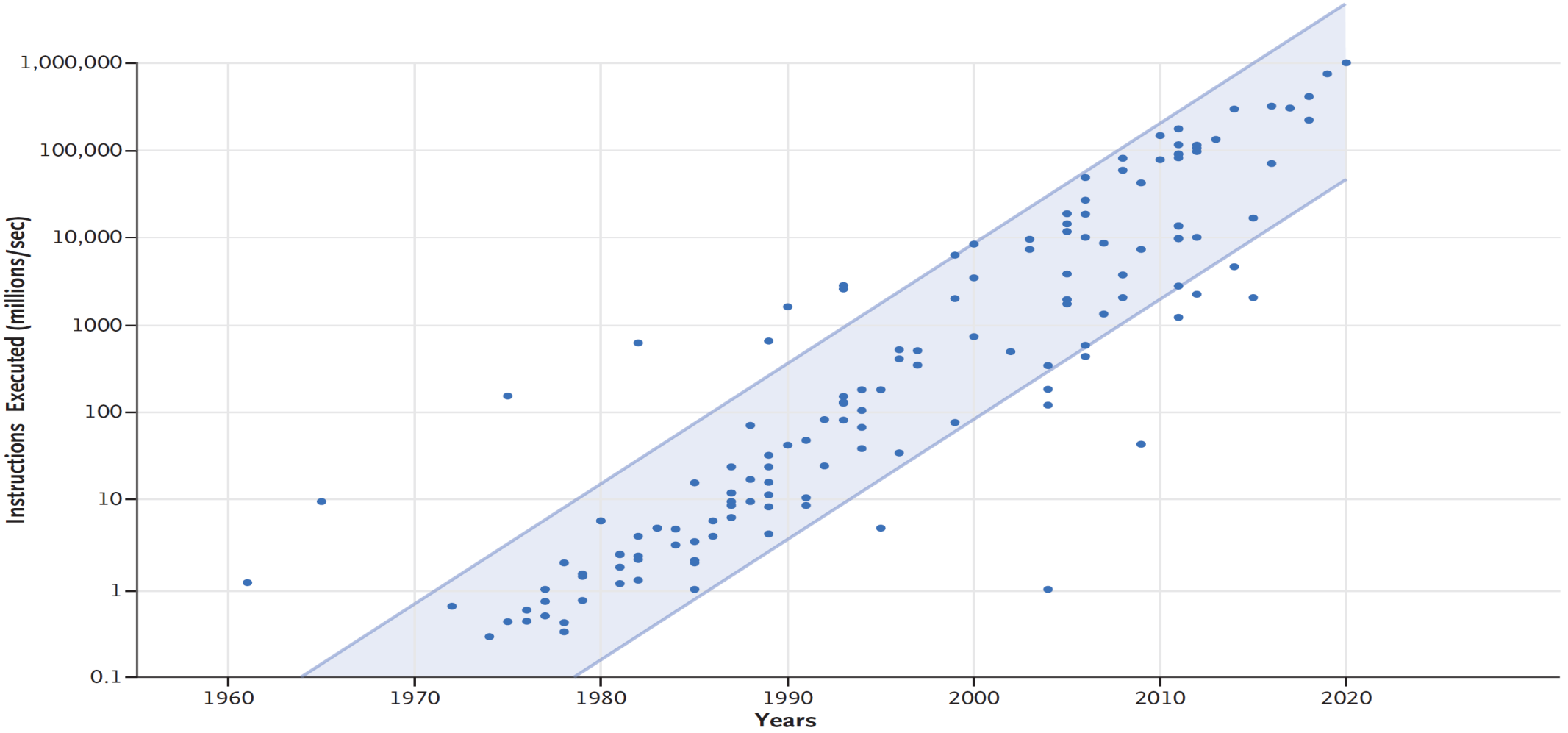

Figure 1. Improvements over 50 Years in the Ability of Computers to Store and Process Data.

Panel A shows advances in data storage, in terms of both physical size and cost per unit of storage. RAMAC denotes random access method of accounting and control. Panel B shows advances in the speed of computing. Each dot represents an individual machine type and the approximate year of its introduction. These improvements in storage and speed have allowed machine learning to progress from a dream to reality. Data in both panels are estimates from many types of system architecture and are derived from multiple public sources.

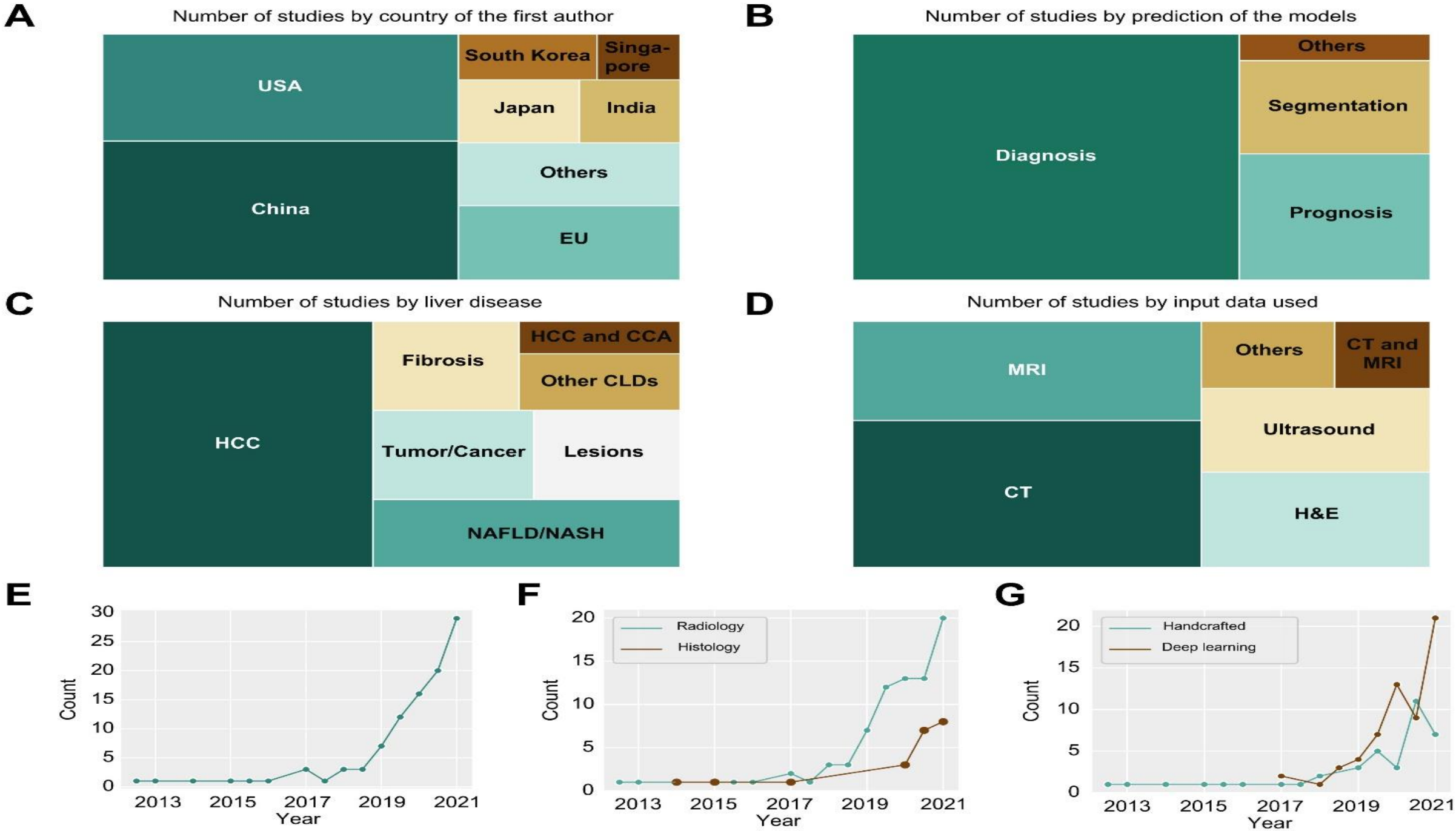
A
Number of studies by country of the first author
USA
South Korea
Singa-pore
Japan
India
China
Others
EU
B
Number of studies by prediction of the models
Diagnosis
Others
Segmentation
Prognosis
C
Number of studies by liver disease
HCC
Fibrosis
HCC and CCA
Other CLDs
Tumor/Cancer
Lesions
NAFLD/NASH
D
Number of studies by input data used
MRI
Others
CT and MRI
Ultrasound
CT
H&E
E
Count
Year
F
Radiology
Histology
Count
Year
G
Handcrafted
Deep learning
Count
Year

Il termine ***Machine Learning*** è stato coniato da Arthur Samuel nel 1959, che lo ha definito come:

> ***«Machine Learning is the field of study that gives computers the ability to learn without being explicitly programmed»***

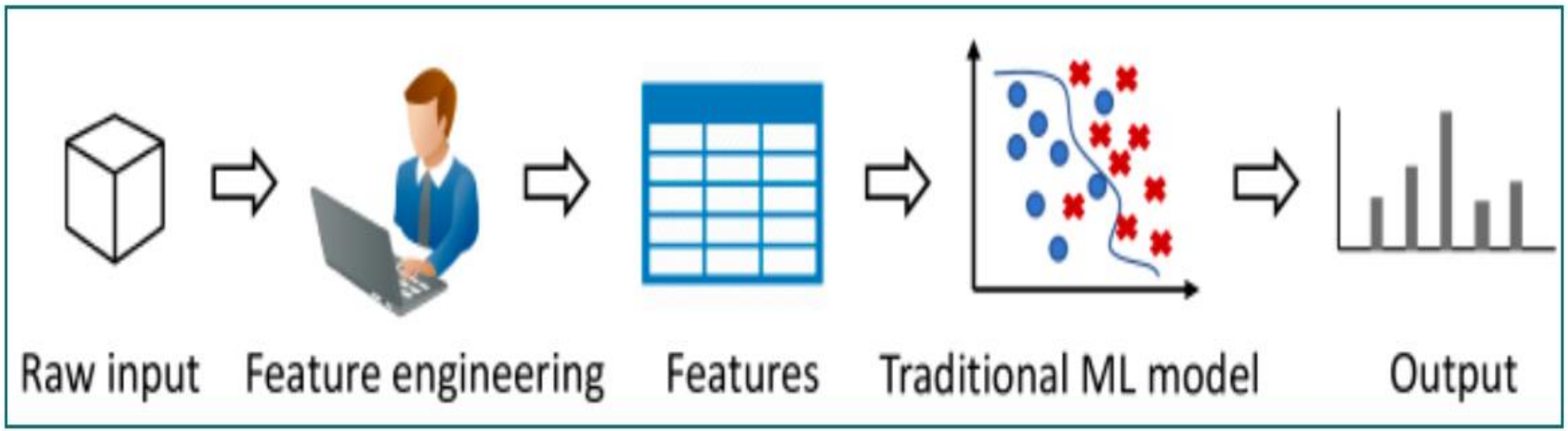

Alcuni compiti non possono essere infatti definiti esaustivamente, tranne che tramite esempi.

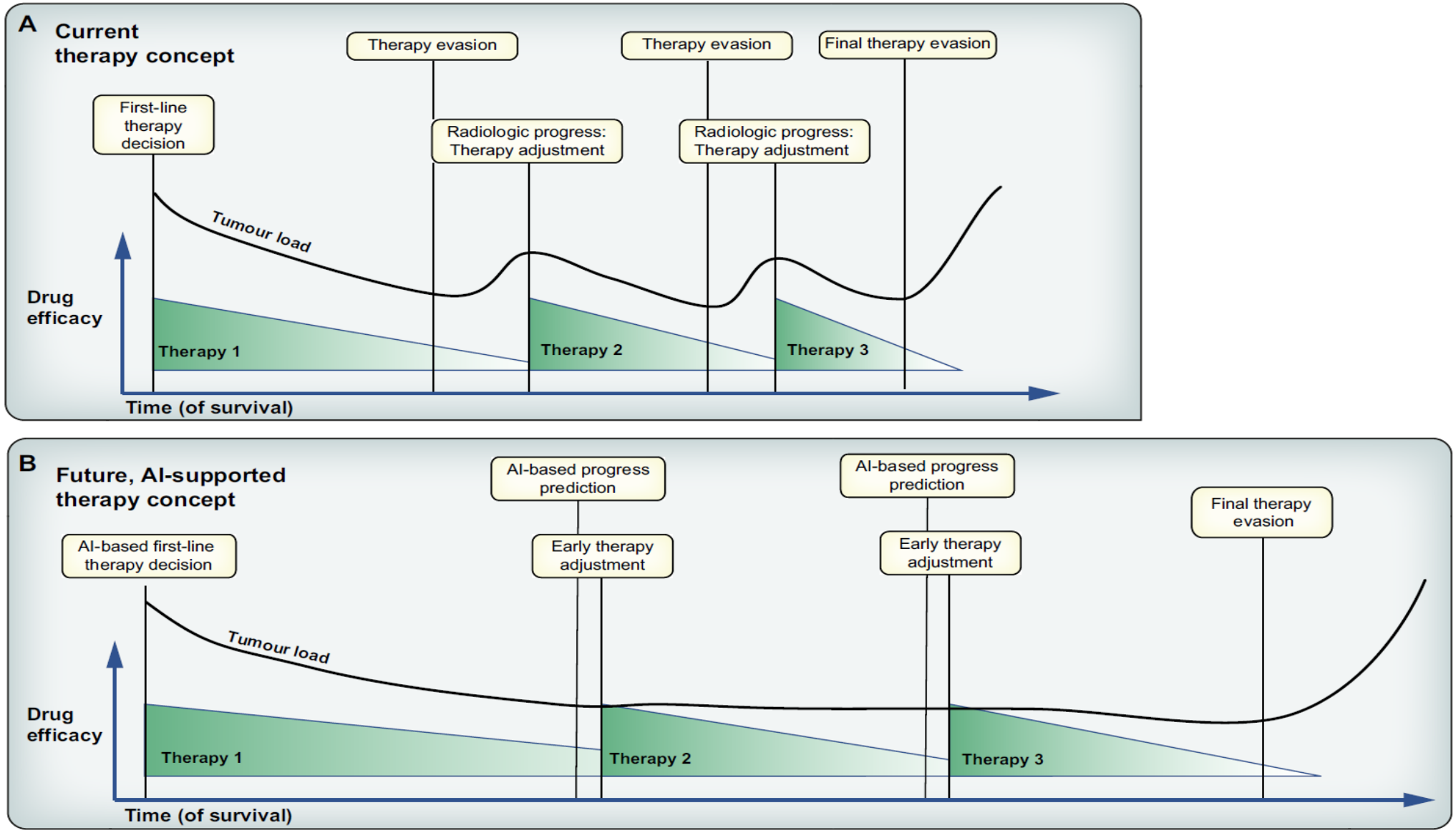

Fig. 4. Artificial intelligence could support doctors in decision making in tumour therapy in the future. (A) Current oncologic therapy pattern. After an initial first-line therapy, the tumour is evading therapy through resistance mechanisms. The following tumour growth is recognised during radiologic follow-up leading to therapy adjustment. (B) Hypothetical, future, AI-supported therapy pattern. Initial, individualized first-line therapy decision, accounting for an AI-based recommendation. After an AI algorithm predicts progression of a tumour, doctors decide to adjust therapy before the tumour can develop resistance to therapy and grow again.

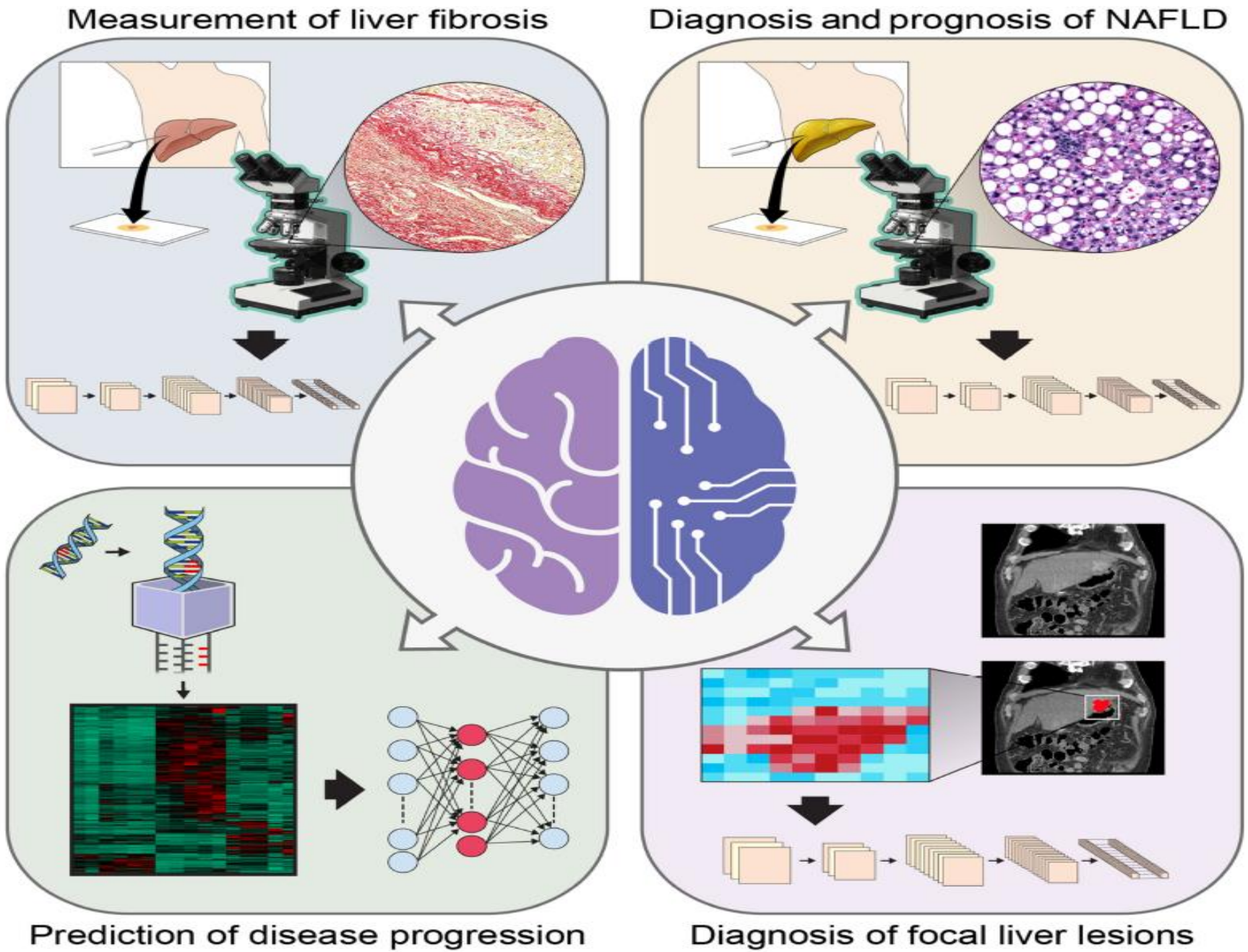
Measurement of liver fibrosis
Diagnosis and prognosis of NAFLD
Prediction of disease progression
Diagnosis of focal liver lesions

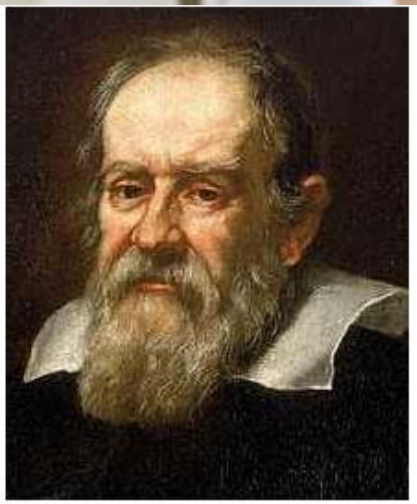

Misura ciò che è misurabile, e rendi misurabile ciò che non lo è

Artificial Intelligence applications in diagnostic and prognostic imaging in hepatology

IMAGING-DRIVEN DIAGNOSIS and PROGNOSIS

IMAGING ACQUISITION **IMAGING INTERPRETATION**

Critical Issues

- **High Subjectivity**
- **Experience and Tiredness**

L’analisi visiva riesce a estrarne solo circa il 10% delle informazioni contenute in una immagine medica digitale

Radiomica = le immagini ottenute dagli esami TAC, RM o PET, vengono convertite in dati numerici.

Se le immagini sono analizzate in dettaglio attraverso dei software di analisi della tessitura dell'immagine è possibile ottenere dati quantitativi oggettivi, in grado di fornire informazioni sui sottostanti fenomeni pato-fisiologici, inaccessibili alla semplice analisi visiva.

Radiogenomica
Mette in relazione i dati quantitativi ottenuti con la radiomica con i dati genomici del tumore.
L’obiettivo è che una semplice analisi radiomica non invasiva possa essere in grado di informarci se un tumore abbia una certa mutazione, evitanto analsi di tessuti !!!!

- La Radiomica è spesso applicata in ambito oncologico, allo scopo di porre le basi per la futura

MEDICINA DI PRECISIONE

Un evidente **vantaggio auspicato** degli approcci radiomici in ambito oncologico è quello di **rimpiazzare la biopsia** del tessuto tumorale, e quindi:

- **sostituire una tecnica invasiva con una non invasiva**;
- **ridurre il rischio di errato campionamento dei tessuti**, dato che negli approcci radiomici l'intera lesione viene analizzata.

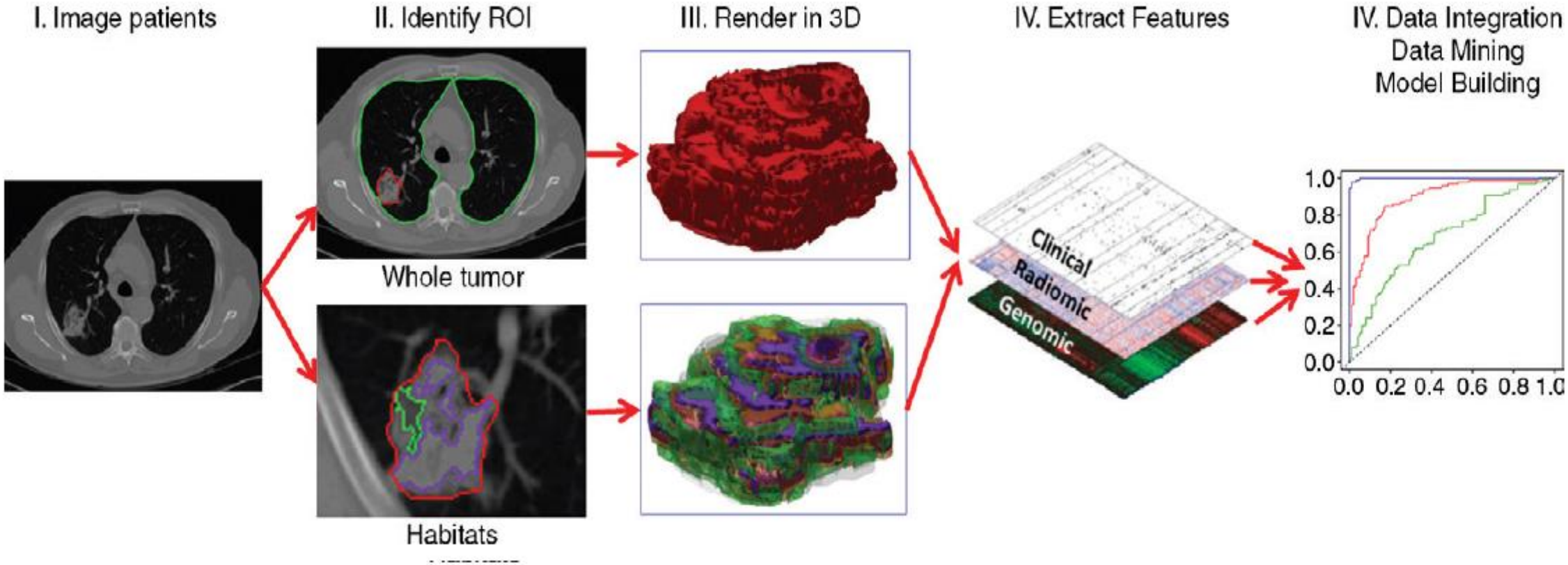

Figure 1: Flowchart shows the process of radiomics and the use of radiomics in decision support. Patient work-up requires information from disparate sources to be combined into a coherent model to describe where the lesion is, what it is, and what it is doing. Radiomics begins with acquisition of high-quality images. From these images, a region of interest *(ROI)* that contains either the whole tumor or subregions (ie, habitats) within the tumor can be identified. These are segmented with operator edits and are eventually rendered in three dimensions *(3D)*. Quantitative features are extracted from these rendered volumes to generate a report, which is placed in a database along with other data, such as clinical and genomic data. These data are then mined to develop diagnostic, predictive, or prognostic models for outcomes of interest.

Radiomics

RADIOMICS: the conversion of digital images into mineable data

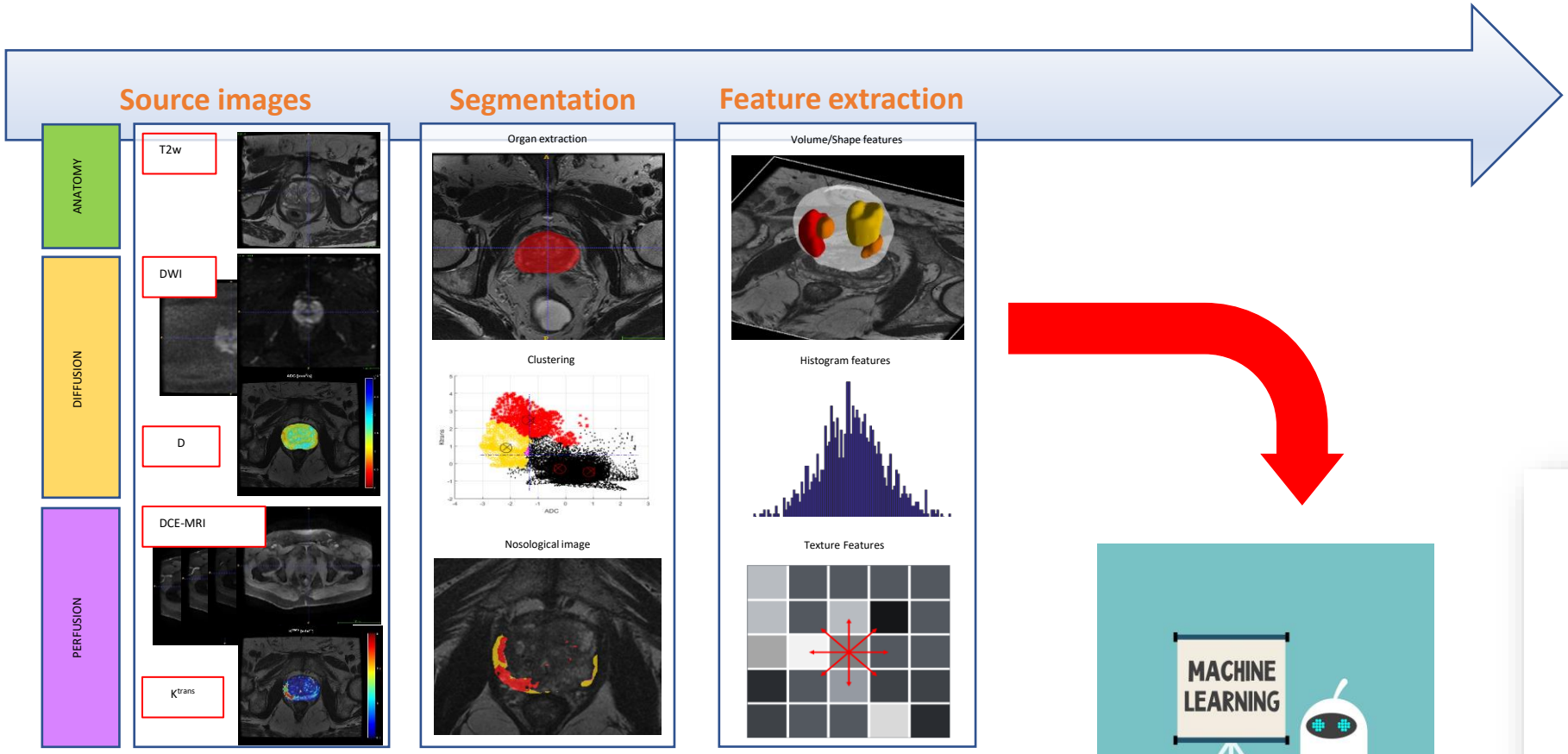

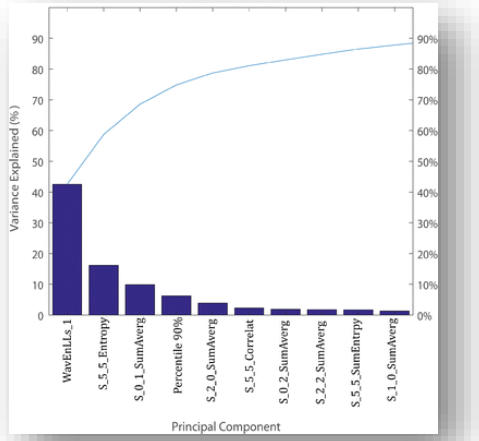

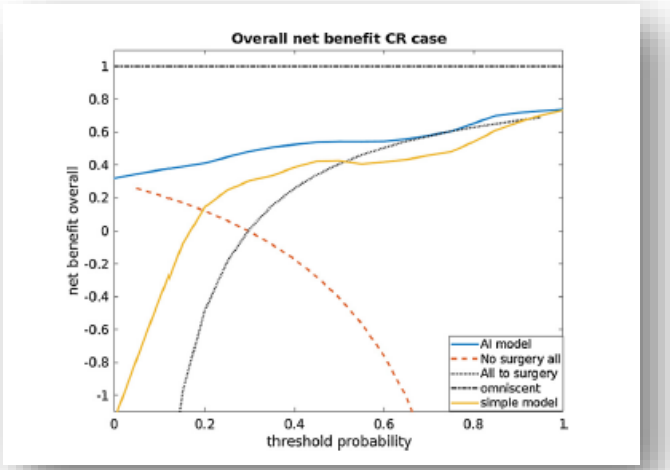

RADIOMIC SIGNATURE

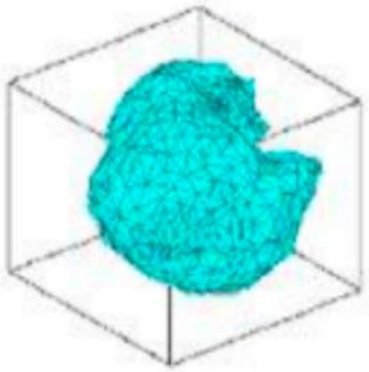

Features relative a forma e dimensione

Features che descrivono forma e dimensione della ROI (2D o 3D).

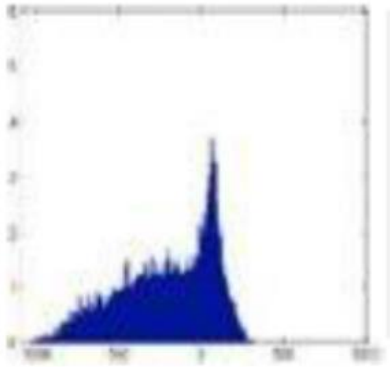

Features statistiche del primo ordine

Features calcolate a partire dall'istogramma che rappresenta la distribuzione dei valori dei pixel/voxel nella ROI.

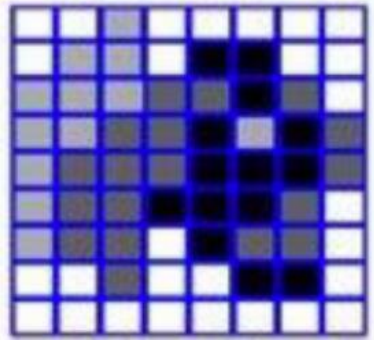

Features statistiche di ordine superiore

Features che descrivono relazioni tra i valori di due o più pixel/voxel nella ROI.

Per effettuare correttamente uno studio di Radiomica + ML è necessario un gruppo di ricerca altamente interdisciplinare, data le molteplici e differenti competenze necessarie:

- Acquisizione dei dati
- Controllo di qualità dei macchinari e dei dati acquisiti
- Segmentazione automatica/manuale delle regioni di interesse
- Annotazione dei campioni
- Preprocessing dei dati
- Estrazione delle features radiomiche
- Addestramento algoritmi di Machine Learning
- Valutazione dei risultati
- Valutazione dell'impatto clinico dei risultati dell'analisi di radiomica + ML

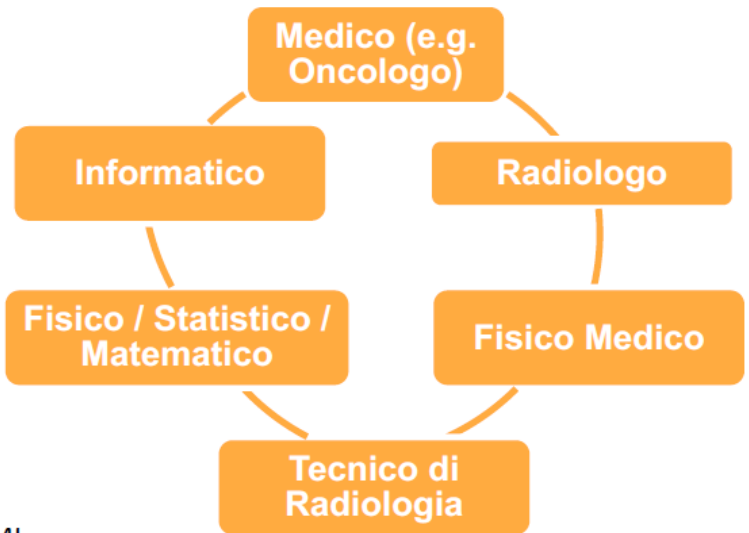

HEAL ITALIA

Health **E**xtended **AL**liance

for

Innovative **T**herapies, **A**dvanced **L**ab-research, and **I**ntegrated **A**pproaches

of Precision Medicine

Tra gli Obiettivi principali:

Sviluppo di algoritmi per

- diagnosi precoce
- modelli di gestione territoriale patologie alto impatto epid.
- stratificazione personalizzata dl rischio di progressione, complicanze e eventi avversi
- benefici ed eventi avversi di terapie farmacologiche
- riposizionamento di farmaci

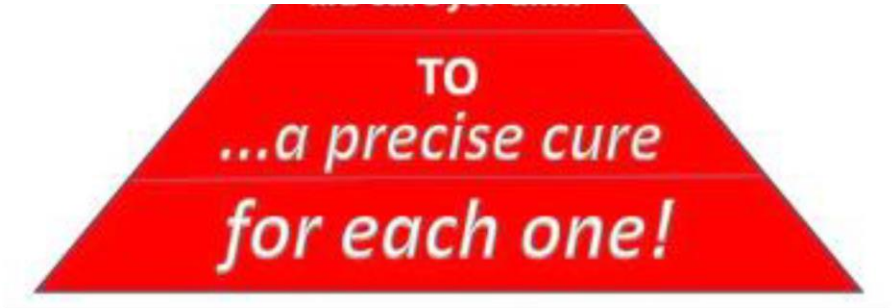

Radiomics: Applicazioni cliniche

Ha diverse applicazioni nell'ambito della diagnostica clinica, tra le quali [1],[2],[3],[4]:

1. Previsione della risposta alla terapia del cancro (Treatment response and Outcomes)
2. Stadiazione del tumore (Tumor staging)
3. Aggressività del tumore (Level of malignancy)
4. Identificazione del tessuto e tipizzazione della lesione (Tissue Identification and typing)
5. Valutazione della genetica del cancro (Radiogenomics)

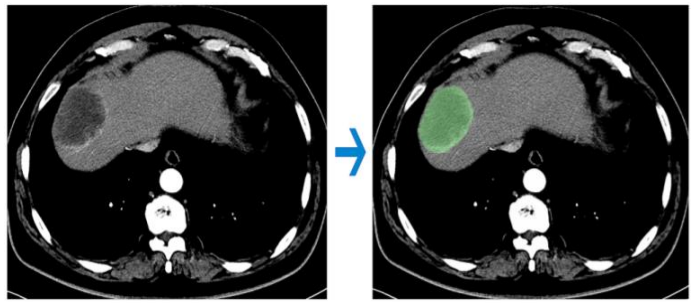

Metastasis linfonodale

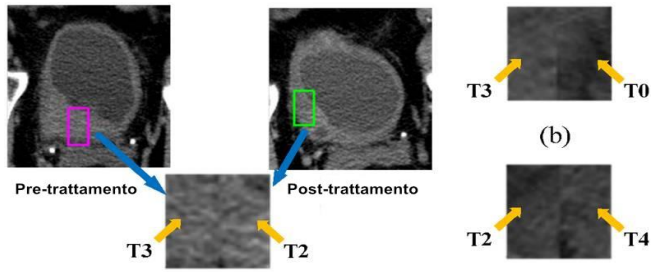

Risposta alla terapia nel cancro della vescica

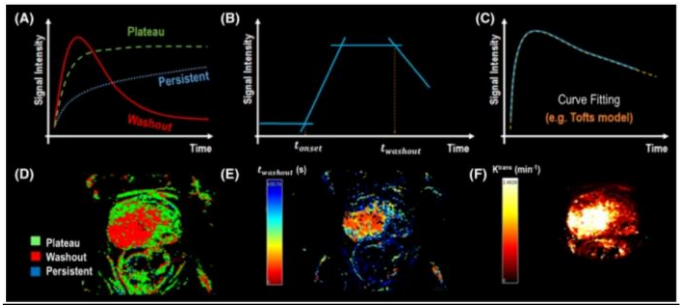

Curve typing

[2] Stephen S F Yip and Hugo J W L Aerts 2016 Phys. Med. Biol. 61 R150
[3] Introduction to Radiomics Marius E. Mayerhoefer, Andrzej Materka, Georg Langs, Ida Häggström, Piotr Szczypiński, Peter Gibbs, Gary Cook Journal of Nuclear Medicine Apr 2020, 61 (4) 488-495
[4] Bogowicz, Marta, et al. "CT radiomics and PET radiomics: ready for clinical implementation?." The Quarterly Journal of Nuclear Medicine and Molecular Imaging: Official Publication of the Italian Association of Nuclear Medicine (AIMN)[and] the International Association of Radiopharmacology (IAR),[and] Section of the Society of.. (2019).

IMAGING INFORMATICS AND ARTIFICIAL INTELLIGENCE

Deep learning for liver tumor diagnosis part I: development of a convolutional neural network classifier for multi-phasic MRI

Charlie A. Hamm[1,2] · Clinton J. Wang[1] · Lynn J. Savic[1,2] · Marc Ferrante[1] · Isabel Schobert[1,2] · Todd Schlachter[1] · MingDe Lin[1] · James S. Duncan[1,3] · Jeffrey C. Weinreb[1] · Julius Chapiro[1] · Brian Letzen[1]

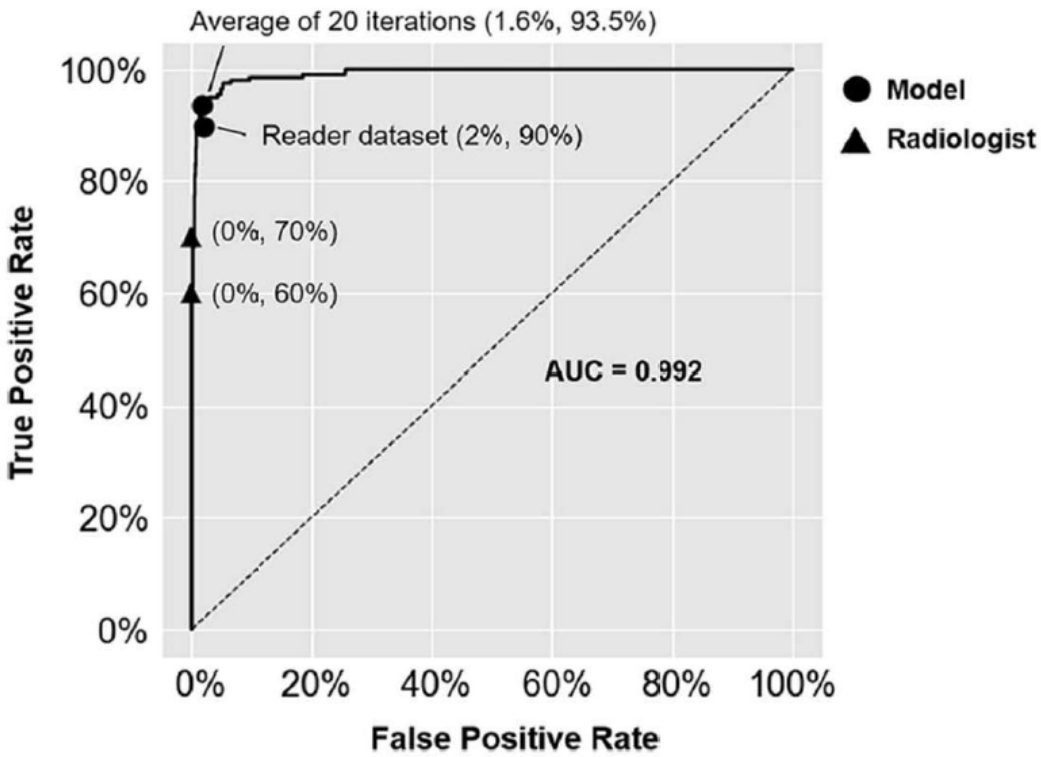

- Four hundred ninety-four hepatic lesions with typical imaging features from six categories(simple cyst, cavernous hemangioma, focal nodular hyperplasia, HCC, intrahepatic cholangiocarcinoma, and colorectal cancer metastasis) were utilized, divided into training (n = 434) and test (n = 60) sets.
- The ground truth was extracted from official reports
- 20 iterations were performed, randomly splitting lesions into training and test set.
- The model performance was evaluated in distinguishing the six lesion entities as well as three broader categories that simulate the application of a deep learning model to an HCC diagnostic imaging framework such as LI-RADS.
- After model engineering was finalized, classification accuracy for the final CNN was compared with two board-certified radiologists on an identical unseen test set

	Accuracy of lesion classification (mean ± SD %)	Accuracy of derived LI-RADS classification (mean ± SD %)	Runtime (mean ± SD)
Average of 20 iterations			
Model training set	98.7 ± 1.0	99.1 ± 0.7	29 min ± 4
Model test set	91.9 ± 2.9	94.3 ± 2.9	5.6 ms ± 4.6
Reader study ($n = 60$)			
Model	90.0	91.7	1.0 ms ± 0.4
Radiologist 1	80.0	88.3	14 ± 10 s
Radiologist 2	85.0	88.3	17 ± 24 s

Academic Radiology
Volume 24, Issue 12, December 2017, Pages 1501-1509

Original Investigation

CT Image-based Decision Support System for Categorization of Liver Metastases Into Primary Cancer Sites: Initial Results

Avi Ben-Cohen MSc [a], Eyal Klang MD [b], Idit Diamant MSc [a], Noa Rozendorn BSc [b], Stephen P. Raskin MD [b], Eli Konen MD [b], Michal Marianne Amitai MD [b], Hayit Greenspan PhD [a]

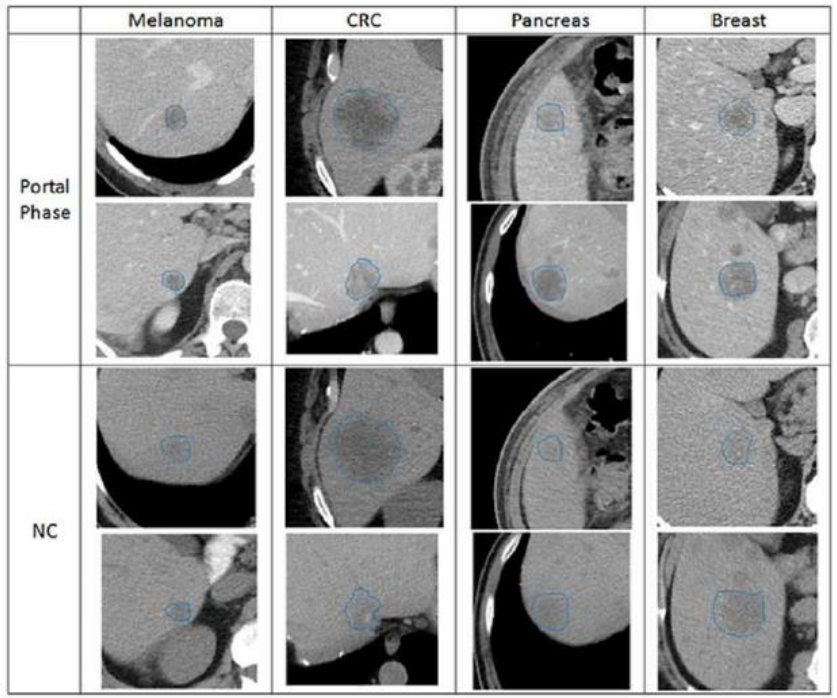

- 50 lesion cases taken from 29 patients were selected for the development set; 142 lesion from 71 patients were chosen for the evaluation set.
- The data include various liver metastatic lesions derived from different primary sites showing melanoma, breast cancer, colorectal cancer, and pancreatic cancer
- For each lesion, two 2D images (portal phase and non contrast CT) were available

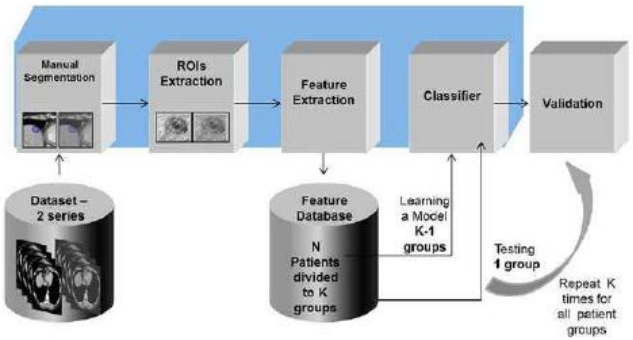

In a multicategory classification task, into the four different primary sites, the first expert achieved a classification accuracy of **42%** and the second expert **33%**

Features	Top-1 ACC	Top-2 ACC	Top-3 ACC
Texture	0.56	0.66	0.90
CNN low-layer selection	0.50	0.66	0.90

Academic Radiology
Volume 24, Issue 12, December 2017, Pages 1501-1509

Original Investigation

CT Image-based Decision Support System for Categorization of Liver Metastases Into Primary Cancer Sites: Initial Results

Avi Ben-Cohen MSc [a], Eyal Klang MD [b], Idit Diamant MSc [a], Noa Rozendorn BSc [b], Stephen P. Raskin MD [b], Eli Konen MD [b], Michal Marianne Amitai MD [b], Hayit Greenspan PhD [a]

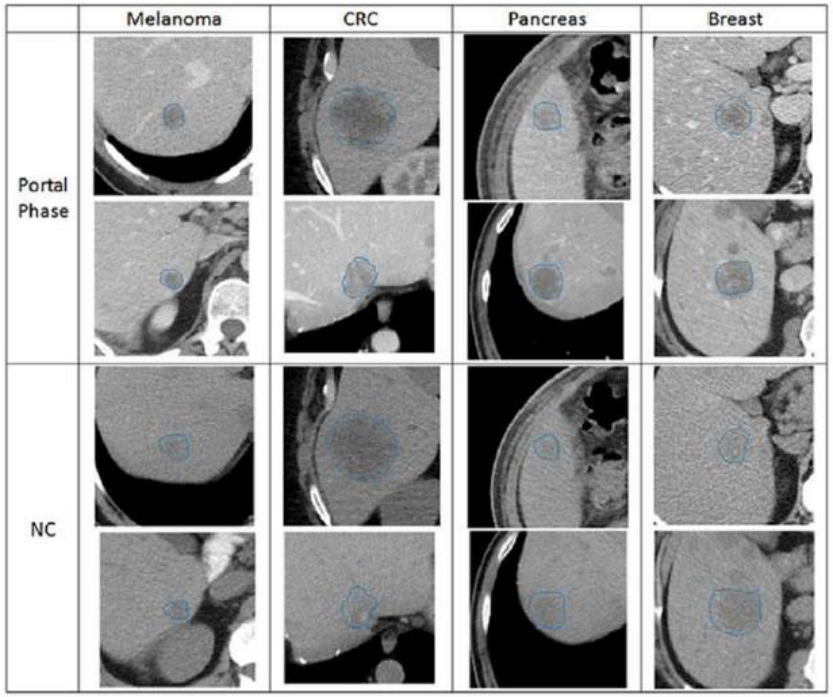

- 50 lesion cases taken from 29 patients were selected for the development set; 142 lesion from 71 patients were chosen for the evaluation set.
- The data include various liver metastatic lesions derived from different primary sites showing melanoma, breast cancer, colorectal cancer, and pancreatic cancer
- For each lesion, two 2D images (portal phase and non contrast CT) were available

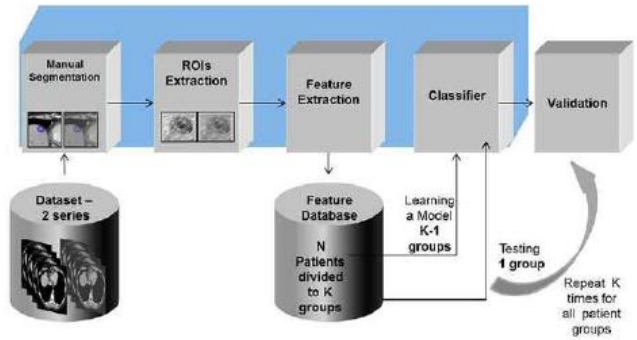

In a multicategory classification task, into the four different primary sites, the first expert achieved a classification accuracy of **42%** and the second expert **33%**

TABLE 4. Top-1, Top-2, and Top-3 Accuracy Results Comparison on the Evaluation Set Using Texture Features, Features Extracted From the CNN, and Age and Gender Information

Features	Top-1 ACC	Top-2 ACC	Top-3 ACC
Age and gender	0.54	0.76	0.94
Texture, age, and gender	0.61	0.81	0.94
CNN low selection and age and gender	0.56	0.83	0.99

Radiomics-Response Prediction

Contents lists available at ScienceDirect

European Journal of Radiology

journal homepage: www.elsevier.com/locate/ejrad

Radiomics diagnosed histopathological growth pattern in prediction of response and 1-year progression free survival for colorectal liver metastases patients treated with bevacizumab containing chemotherapy

- **119 affected by liver metastases in CRC treated with bevacizumab**
- **Manually 3D segmentation on non-contrast CT phase**
- **Radiomics model designed to identify histophatologic growth pattern**
- **To predict early response**
- **To predict 1-year PFS**

Radiomics in early response:
- **AUC 0.707 per-lesion, AUC 0.720 per-patient**

Radiomics 1-year PFS:
- **Was the only indipendent predictor of 1-year PFS**

Univariable and Multivariable Cox Proportional Hazards Models for 1-Year Progression-Free Survival.

Covariate	Univariable analysis		Multivariable analysis	
	HR (95% CI)	*P* value	HR (95% CI)	*P* value
RAD_HGP	0.339 (0.176–0.655)	0.001	0.396 (0.195–0.804)	0.010
ER_PVP	0.561 (0.314–1.001)	0.050		
Liver resection	0.247 (0.060–0.018)	0.053		
Morphologic response	0.268 (0.268–0.846)	0.011	0.676 (0.365–1.253)	0.214

Wei S I et al., EJR 2021

histopathologic growth pattern (HGP)

Radiomics-Response Prediction

LIVER METS

OXFORD

JNCI J Natl Cancer Inst (2020) 112(9): djaa017

doi: 10.1093/jnci/djaa017
First published online February 4, 2020
Article

Radiomics Response Signature for Identification of Metastatic Colorectal Cancer Sensitive to Therapies Targeting EGFR Pathway

- **667 metasta**
- **Segmentati**
  - 3499 features
- **To predict tumor sensitivities to CHT**

Radiomics-derived support tools could give clinicians an early prediction of the success of treatment with FC using conventional standard-of-care CT scans

	Anti-EGFR treatment		No anti-EGFR treatment	
	FOLFIRI + cetuximab		FOLFIRI only	
	mCRC		mCRC	
Analysis	CRC-FC^{HQ}	CRC-FC^{SD}	CRC-F^{HQ}	CRC-F^{SD}
Reference standard	OS	OS	OS	OS
No. patients				
Total	116	186	129	236
Training	78	124	78	159
Sensitive	48	71	42	85
Resistant	30	53	36	74
Validation	38	62	51	78
				42
				36
				Random Forest
				Shape SI4
				LoG Z Entropy
				GTDM Contrast
				LoG X Entropy
Performance				
Tumor sensitivity	OS >17.7 mo	OS >17.7 mo	OS >17.7 mo	OS >17.7 mo
AUC, training	0.83 (95% CI = 0.75 to 0.95)	0.84 (95% CI = 0.76 to 0.89)	0.75 (95% CI = 0.63 to 0.85)	0.75 (95% CI = 0.67 to 0.82)
AUC, validation	0.80 (95% CI = 0.69 to 0.94)	0.72 (95% CI = 0.59 to 0.83)	0.59 (95% CI = 0.44 to 0.72)	0.55 (95% CI = 0.43 to 0.66)
Association with OS				
Cox regression				
Hazard ratio	44.3 (95% CI = 6.4 to 307.7)	6.5 (95% CI = 1.8 to 23.6)	1.9 (95% CI = 0.4 to 8.4)	0.96 (95% CI = 0.2 to 4.3)
Death	31/38	53/62	42/51	69/78
P	.0001	.005	.43	.96

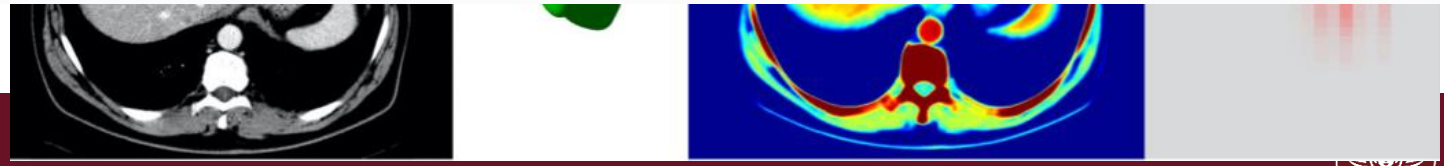

Dercle L et al., JNCI 2020

Radiomics-Response Prediction

diagnostics

MDPI

Article

Assessment of Response to Chemotherapy in Pancreatic Cancer with Liver Metastasis: CT Texture as a Predictive Biomarker

AIM: To test CT texture of metastatic in comparison with RECIST 1.1, Choi and modified Choi criteria in evaluating treatment and determining time to progression (TTP) in metastatic PDAC

5. Conclusions

Our findings indicated that the existing assessment criteria, including RECIST 1.1, Choi and modified Choi, were not sufficient for the evaluation of tumor response to treatment. We found that the percentage change in texture SD of liver metastatic lesions derived from contrast-enhanced CT texture analysis, might better predict tumor response and TTP in pancreatic patients with liver metastasis undergoing chemotherapy. Therefore, CT texture was proved to be an effective assessment tool and biomarker that predicted tumor response and TTP in a manner that was superior to traditional response criteria based on enhancement change, size change, or both.

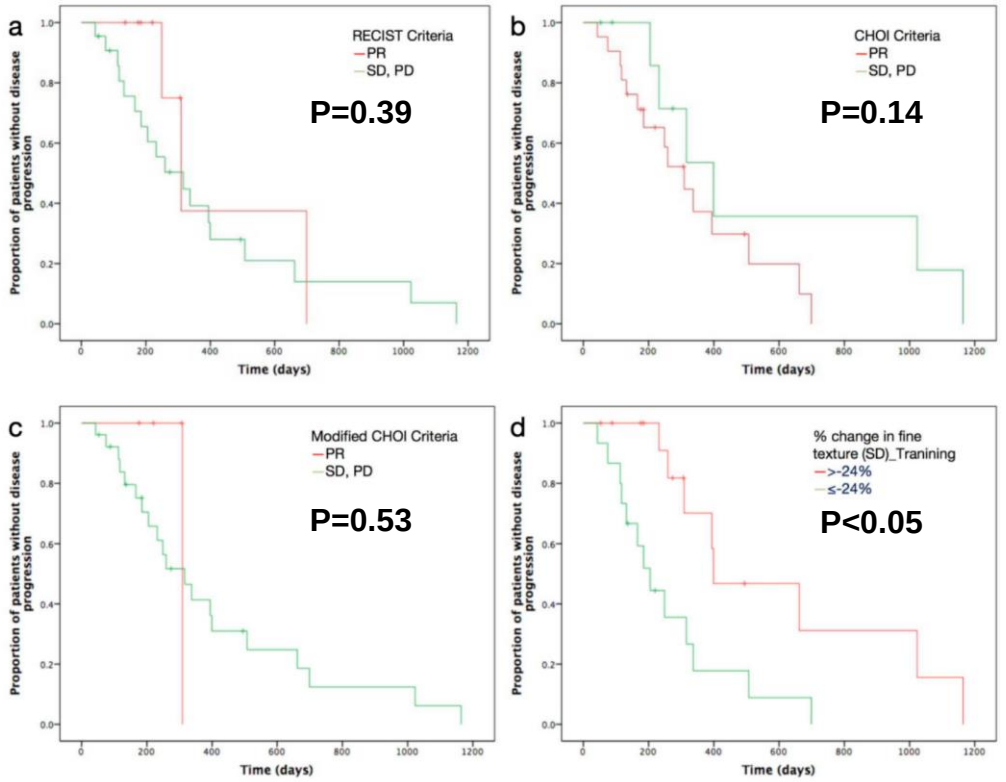

Cox regression analysis showed:

- **percentage change in SD was an independent predictor of TTP (p = 0.016)**
- **confirmed in the validation cohort (p = 0.019)**

Cheng et al., Diagnostics 2021

In this paper, we assess changes in CT texture of metastatic liver lesions after treatment with chemotherapy in patients

RESEARCH ARTICLE Open Access

CT-based peritumoral radiomics signatures to predict early recurrence in hepatocellular carcinoma after curative tumor resection or ablation

Quan-yuan Shan[1], Hang-tong Hu[1], Shi-ting Feng[2], Zhen-peng Peng[2], Shu-ling Chen[1], Qian Zhou[3], Xin Li[4], Xiao-yan Xie[1], Ming-de Lu[1,5], Wei Wang[1*] and Ming Kuang[1,5*]

- A prediction model based on peritumoral radiomics signatures from pretreatment CT images was constructed to predict early recurrence of HCC after curative treatment.
- 156 patients randomly divided into training cohort (109 patients) and validation cohort (47 patients).
- Early recurrence was defined as the presence of new intrahepatic lesions or metastasis with typical imaging features of HCC, or atypical findings with histopathological confirmation within 2 years after curative resection or ablation of HCC.
- A region of interest (ROI) was manually delineated around the lesion for tumoral radiomics (T-RO) feature extraction, and another ROI was outlined with an additional 2 cm peritumoral area for peritumoral radiomics (PT-RO) feature extraction.
- The T-RO and PT-RO models were constructed using LASSO logistic regression and compared to the peritumoral Enhancement (PT-E) detected by a radiologist.

Models	AUC		cfNRI			IDI		PPV		NPV	
	AUC [95%CI]	P	cfNRI+	cfNRI-	P	IDI	P	PPV	P	NPV	P
PT-RO	0.79 [0.66, 0.92]	–	–	–	–	–	–	0.93	–	0.64	–
T-RO	0.62 [0.46, 0.79]	< 0.01	−0.47	−0.32	< 0.01	0.22	< 0.01	0.63	< 0.01	0.65	0.92
PT-E	0.61 [0.47, 0.74]	< 0.01	−0.24	−0.41	0.02	0.20	0.01	0.69	< 0.01	0.55	0.38

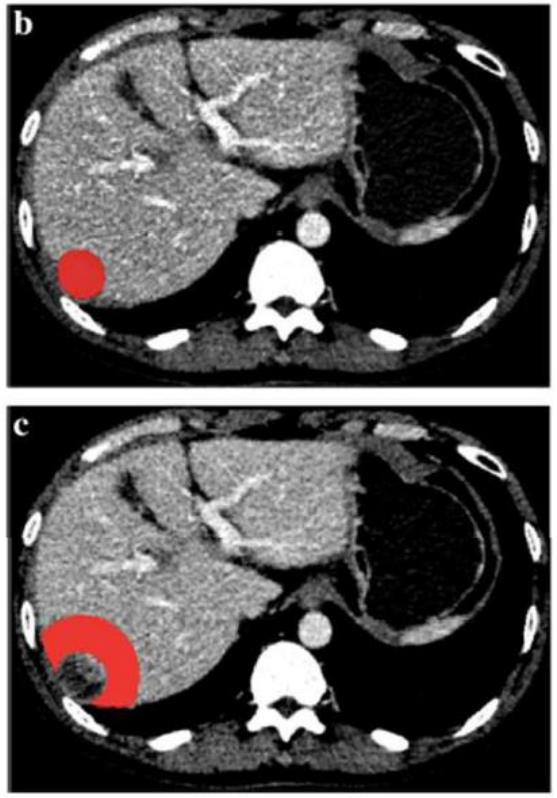

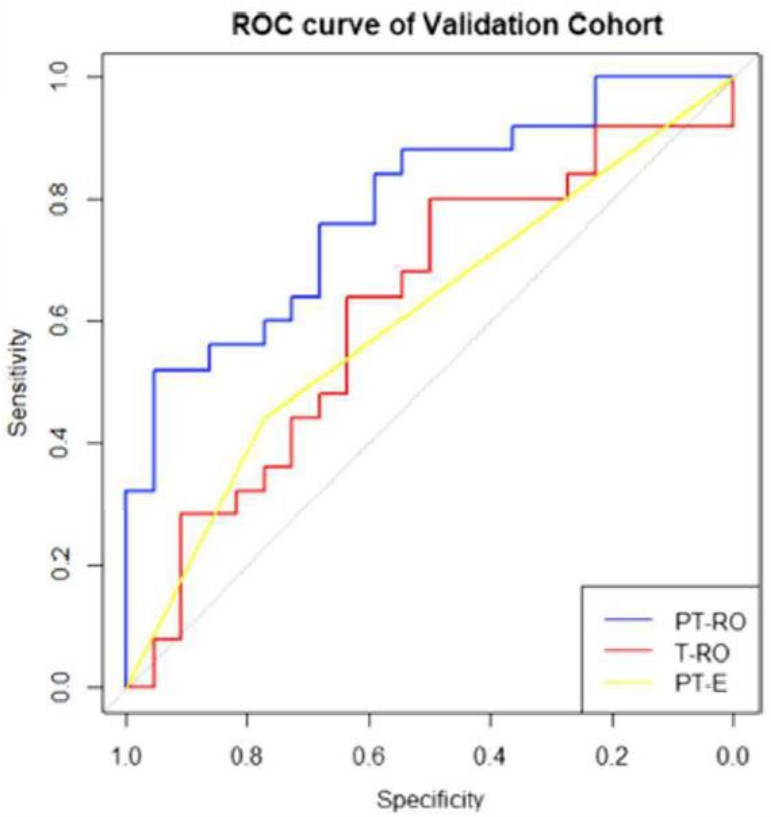

umor. A region of interest (ROI) was manually delineated around the lesion for tumoral radiomics (T-RO) feature extraction, and another ROI was outlined with an additional 2 cm peritumoral area for peritumoral radiomics (PT-

Radiomics and CCA

First author [Ref.]	Year	Images	Methods	Subjects, *n*	Purpose	AUC
Matake et al. [104]	2006	CECT	ANN	120	To evaluate the performance of ANN for differential diagnosis of hepatic masses, including CCA	0.961
Logeswaran [25]	2009	MRCP	MLP	648	To differentiate images with CCA from those without	–
Pattanapairoj et al. [26]	2015	No	C4.5, ANN	85	To improve the diagnostic power of serum markers using C4.5 and ANN	–
Sadot et al. [27]	2015	CECT	Multiple linear regression analysis	56	To investigate associations between imaging features of CCA and texture analysis	–
Liang et al. [28]	2018	CECT	LASSO	209	To develop a novel radiomics nomogram for predicting ER of ICC	0.90
Shao et al. [105]	2018	No	BP-ANN	288	To predict early occlusion of bilateral plastic stent placement for inoperable HCC	0.9648
Ji et al. [106]	2019	CECT	LASSO	103	To develop a radiomics model for predicting LNM of ICC and to determine its prognostic value	0.9244
Ji et al. [107]	2019	CECT	LASSO	247	To evaluate a radiomics model for predicting LNM in BTCs and to determine its prognostic value	0.81
Xu et al. [108]	2019	MRI	SVM	148	To develop a prediction model for preoperative LNM in ICC patients	0.870
Peng et al. [109]	2019	US	LASSO, SVM	128	To develop radiomics signatures based on US to assess the biological behaviors of ICC	0.930
Yang et al. [110]	2020	MRI	Random forest	100	To evaluate diagnostic performance of radiomics models of MRI in the detection of DD and LNM of ECC	0.90

Yang et al. Oncology 2021

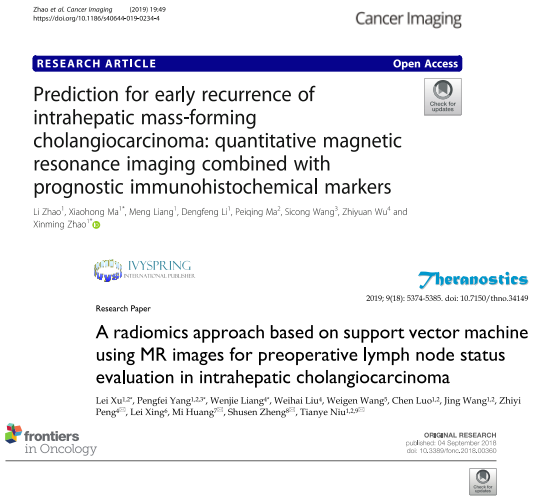
Cancer Imaging

RESEARCH ARTICLE Open Access

Prediction for early recurrence of intrahepatic mass-forming cholangiocarcinoma: quantitative magnetic resonance imaging combined with prognostic immunohistochemical markers

Li Zhao, Xiaohong Ma, Meng Liang, Dengfeng Li, Peiqing Ma, Sicong Wang, Zhiyuan Wu and Xinming Zhao

Theranostics

Research Paper

A radiomics approach based on support vector machine using MR images for preoperative lymph node status evaluation in intrahepatic cholangiocarcinoma

frontiers in Oncology

ORIGINAL RESEARCH

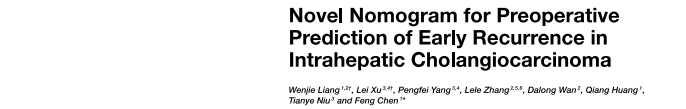
Novel Nomogram for Preoperative Prediction of Early Recurrence in Intrahepatic Cholangiocarcinoma

Wenjie Liang, Lei Xu, Pengfei Yang, Lele Zhang, Dalong Wan, Qiang Huang, Tianye Niu and Feng Chen

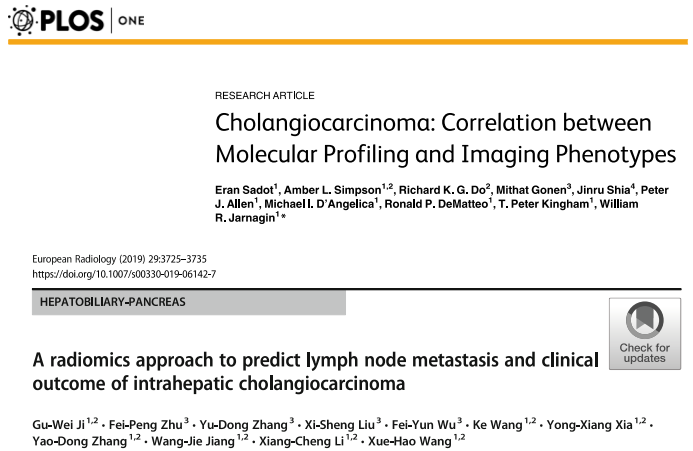
PLOS ONE

RESEARCH ARTICLE

Cholangiocarcinoma: Correlation between Molecular Profiling and Imaging Phenotypes

Eran Sadot, Amber L. Simpson, Richard K. G. Do, Mithat Gonen, Jinru Shia, Peter J. Allen, Michael I. D'Angelica, Ronald P. DeMatteo, T. Peter Kingham, William R. Jarnagin

European Radiology (2019) 29:3725–3735

HEPATOBILIARY-PANCREAS

A radiomics approach to predict lymph node metastasis and clinical outcome of intrahepatic cholangiocarcinoma

Gu-Wei Ji · Fei-Peng Zhu · Yu-Dong Zhang · Xi-Sheng Liu · Fei-Yun Wu · Ke Wang · Yong-Xiang Xia · Yao-Dong Zhang · Wang-Jie Jiang · Xiang-Cheng Li · Xue-Hao Wang

Radiomics and CCA

European Radiology
https://doi.org/10.1007/s00330-020-07250-5

COMPUTED TOMOGRAPHY

Radiomics using CT images for preoperative prediction of futile resection in intrahepatic cholangiocarcinoma

Hongpeng Chu[1] · Zelong Liu[2] · Wen Liang[3] · Qian Zhou[4] · Ying Zhang[1] · Kai Lei[1] · Mimi Tang[5] · Yiheng Cao[4] · Shuling Chen[2] · Sui Peng[4,6] · Ming Kuang[1,2]

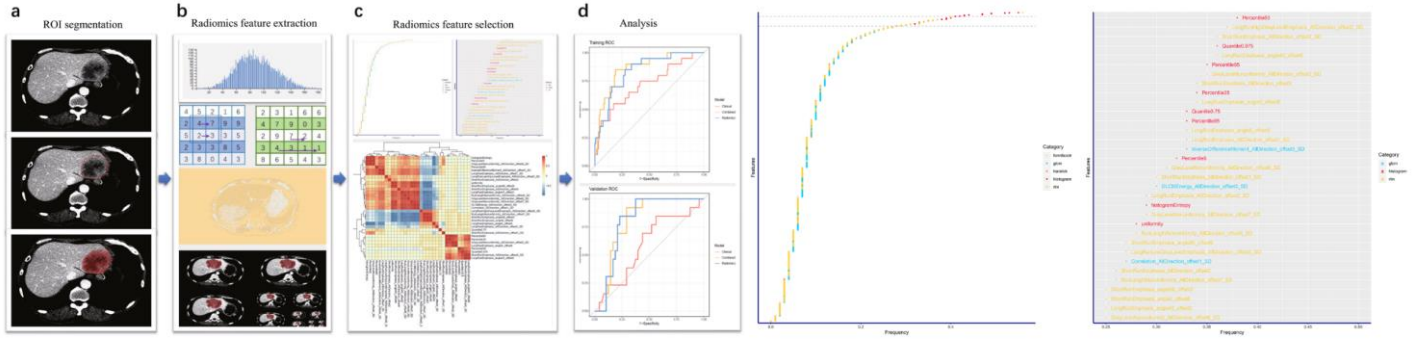

Table 2 Performance of three prediction models: the clinical model, the radiomics model, and the combined model

	Group	Radiomics	Clinical	Combined model
AUC (95% CI)	training	0.838 (0.751, 0.924)	0.716 (0.582, 0.849)	0.864 (0.781, 0.947)
	Validation	0.804 (0.697, 0.912)	0.59 (0.415, 0.765)	0.8 (0.69, 0.909)
Accuracy (95% CI)	training	0.739 (0.659, 0.809)	0.683 (0.6, 0.759)	0.817 (0.743, 0.877)
	Validation	0.787 (0.663, 0.881)	0.59 (0.457, 0.714)	0.754 (0.627, 0.855)
Sensitivity (95% CI)	training	0.85 (0.621, 0.968)	0.65 (0.408, 0.846)	0.85 (0.621, 0.968)
	Validation	0.846 (0.546, 0.981)	0.692 (0.386, 0.909)	0.923 (0.64, 0.998)
Specificity (95% CI)	training	0.721 (0.633, 0.799)	0.689 (0.598, 0.769)	0.811 (0.731, 0.877)
	Validation	0.771 (0.627, 0.88)	0.562 (0.412, 0.705)	0.708 (0.559, 0.83)
NPV (95% CI)	training	0.967 (0.907, 0.993)	0.923 (0.848, 0.969)	0.971 (0.916, 0.994)
	Validation	0.949 (0.827, 0.994)	0.871 (0.702, 0.964)	0.971 (0.851, 0.999)
PPV (95% CI)	training	0.333 (0.208, 0.479)	0.255 (0.143, 0.396)	0.425 (0.27, 0.591)
	Validation	0.5 (0.282, 0.718)	0.3 (0.147, 0.494)	0.462 (0.266, 0.666)

Table 1 Baseline clinical characteristics of the training and validation cohort

Variables	Levels	Total	Training	Validation	*p* value
n		203	142	61	
Age, years		58.00 [51.00, 67.00]	57.00 [50.00, 66.00]	59.00 [54.00, 68.00]	0.169
Gender	Male	105 (51.7)	71 (50.0)	34 (55.7)	0.551
	Female	98 (48.3)	71 (50.0)	27 (44.3)	
History of previous cholelithiasis	No	174 (85.7)	120 (84.5)	54 (88.5)	0.595
	Yes	29 (14.3)	22 (15.5)	7 (11.5)	
Liver cirrhosis	No	201 (99.0)	140 (98.6)	61 (100.0)	1.000
	Yes	2 (1.0)	2 (1.4)	0 (0.0)	
History of previous liver surgery	No	192 (94.6)	134 (94.4)	58 (95.1)	1.000
	Yes	11 (5.4)	8 (5.6)	3 (4.9)	
CT reports					
Tumor size, mm, mean ± SD		63.4 ± 27.2	64.60 ± 27.56	60.61 ± 26.19	0.338
Number of tumor	0*	2 (1.0)	1 (0.7)	1 (1.6)	0.811
	1	160 (78.8)	114 (80.3)	46 (75.4)	
	2	13 (6.4)	8 (5.6)	5 (8.2)	
	3	3 (1.5)	2 (1.4)	1 (1.6)	
	> 3	25 (12.3)	17 (12.0)	8 (13.1)	
Tumor boundary	Not sure	32 (15.8)	18 (12.7)	14 (23.0)	0.164
	clear	22 (10.8)	15 (10.6)	7 (11.5)	
	obscure	149 (73.4)	109 (76.8)	40 (65.6)	
Bile duct stone	No	148 (72.9)	103 (72.5)	45 (73.8)	0.993
	Yes	55 (27.1)	39 (27.5)	16 (26.2)	
Bile duct dilatation	No	104 (51.2)	70 (49.3)	34 (55.7)	0.491
	Yes	99 (48.8)	72 (50.7)	27 (44.3)	
Bile duct invasion	No	178 (87.7)	124 (87.3)	54 (88.5)	0.995
	Yes	25 (12.3)	18 (12.7)	7 (11.5)	
Lymph node metastasis	No	119 (58.6)	82 (57.7)	37 (60.7)	0.818
	Yes	84 (41.4)	60 (42.3)	24 (39.3)	
Adjacent tissue invasion	No	193 (95.1)	135 (95.1)	58 (95.1)	1.000
	Yes	10 (4.9)	7 (4.9)	3 (4.9)	
Ascites	No	197 (97.0)	137 (96.5)	60 (98.4)	0.671
	Yes	6 (3.0)	5 (3.5)	1 (1.6)	
Cirrhosis	No	192 (94.6)	134 (94.4)	58 (95.1)	1.000
	Yes	11 (5.4)	8 (5.6)	3 (4.9)	
Splenomegaly	No	180 (88.7)	124 (87.3)	56 (91.8)	0.495
	Yes	23 (11.3)	18 (12.7)	5 (8.2)	
Time between CT and surgery		6 (4.00, 10.00)	7 [4.00, 10.75]	6 [3.00, 8.00]	0.194
Laboratory data					
HbsAg	Positive	160 (78.8)	117 (82.4)	43 (70.5)	0.086
	Negative	43 (21.2)	25 (17.6)	18 (29.5)	
WBC, 10^9 /L		7.33 [5.86, 9.14]	7.41 [6.00, 9.12]	7.18 [5.40, 9.16]	0.458
NLR		2.62 [1.87, 3.84]	2.72 [2.03, 4.07]	2.49 [1.67, 3.40]	0.045
Hb, g/L		40.10 [36.65, 42.90]	39.95 [36.50, 42.57]	40.50 [37.40, 43.30]	0.462
Total bilirubin, μmol/L		12.10 [9.30, 17.00]	12.15 [9.40, 16.68]	12.10 [9.20, 18.80]	0.953
Direct bilirubin, μmol/L		3.00 [2.10, 4.70]	2.90 [2.00, 4.59]	3.50 [2.20, 5.00]	0.193
ALT, U/L		25.00 [16.50, 47.50]	24.00 [15.25, 43.50]	28.00 [19.40, 60.00]	0.081
AST, U/L		28.00 [23.90, 42.35]	28.00 [22.25, 42.75]	29.00 [25.00, 41.30]	0.541
PT, s		11.90 [11.40, 12.60]	11.90 [11.40, 12.80]	11.80 [11.40, 12.40]	0.275
AFP, μg/L		3.49 [2.42, 5.63]	3.20 [2.34, 5.39]	3.98 [2.71, 7.21]	0.038
CEA, ng/mL		3.23 [1.95, 9.83]	3.16 [1.81, 10.03]	3.25 [2.03, 8.45]	0.812
CA19_9, U/mL		64.57 [14.03, 1020.23]	78.39 [14.46, 1009.90]	40.86 [13.81, 1779.80]	0.631
Surgical outcome					
Futile	No	170 (83.7)	122 (85.9)	48 (78.7)	0.201
	Yes	33 (16.3)	20 (14.1)	13 (21.3)	

AI and Liver Cancer

Detection/Diagnosis of focal liver lesions

Task	Type	Accuracy	Ref
Predicting the primary origin of liver metastasis	Radiomics and Deep learning based on CT	56%	*Ben Cohen A, 2017*
Detecting liver new tumors	Deep learning based on CT	86%	*Vivanti R, 2017;*
Detecting focal liver lesions	Deep learning based on ultrasound	89%	*Tiyarattanachai T, 2021*
Detecting liver tumors	Deep learning based on MRI	90%	*Kim J, 2020*
Detecting and distinguishing different focal liver lesions.	Deep learning based on ultrasound	97.2%	*Hassan TM, 2017*
Detecting metastatic liver malignancy	Deep learning based on PET/CT	90.5%	*Preis O, 2011*
Evaluating focal liver lesion	Deep learning based on MRI	92%	*Hamm C, 2019*
Evaluating focal liver lesion	Deep learning based on CT	84%	*Yasaka K, 2018*

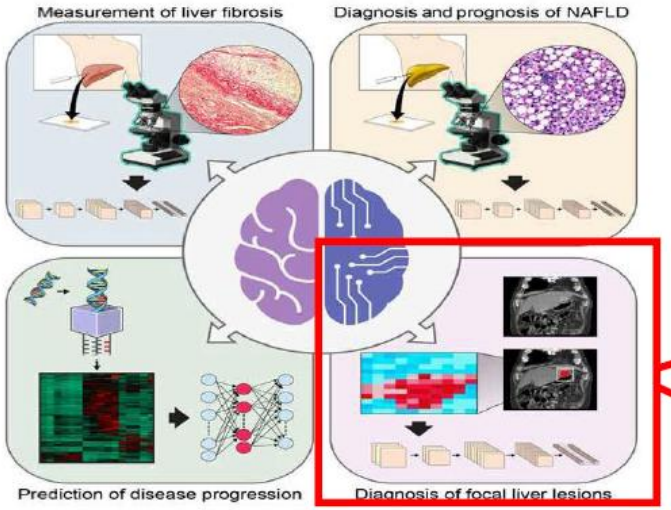

Focal liver lesion **detection**

Focal liver lesion **evaluation**

CLINICAL IMPACT ON LIVER IMAGING

DIFFUSE LIVER DISEASES

- Non-contrast-enhanced CT texture analysis predicted **non-alcoholic steatohepatitis**
- Deep learning system allows for accurate staging of liver **fibrosis** by using enhanced CT images
- Diagnose clinically significant **portal hypertension** and predict **esophageal varices severity**

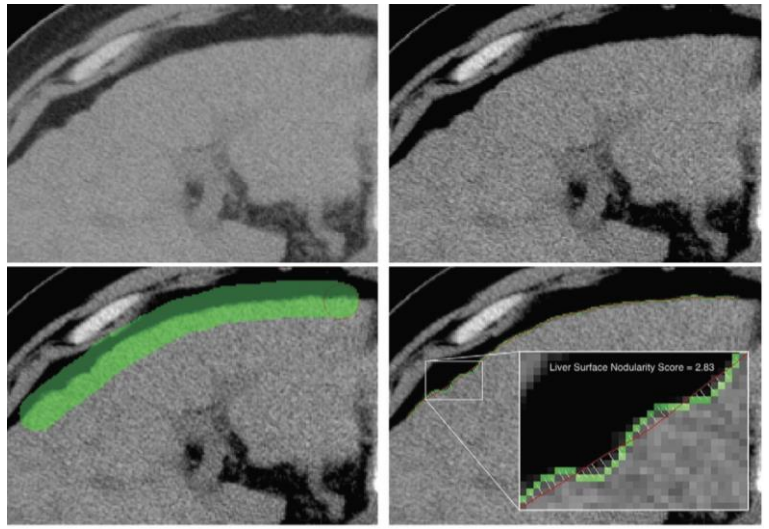

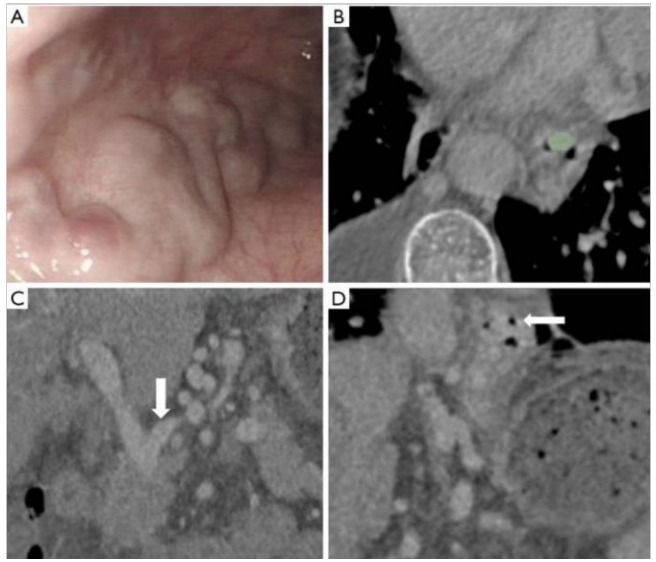

Liu F. et al. E. bio. Medicine 2018
Wan s. et al. Ann. Transl. Med. 2020

AI and Liver Fibrosis

Measurement of liver fibrosis

Type	AUC Cirrhosis	AUC Advanced fibrosis	AUC significant fibrosis	Ref
Deep learning based on contrast enhanced MRI	0.84	0.84	0.85	*Yasaka K, 2017*
Deep learning based on contrast enhanced CT	0.95	0.97	0.96	*Choi K J, 2018*
Deep learning based on shear wave elastography	0.97	0.98	0.85	*Wang K, 2019*
Deep learning based on ultrasound	0.90	-	0.90	*Lee J H, 2019*
Radiomics based on contrast enhanced MRI	0.87	0.88	0.91	*Park H J, 2019*

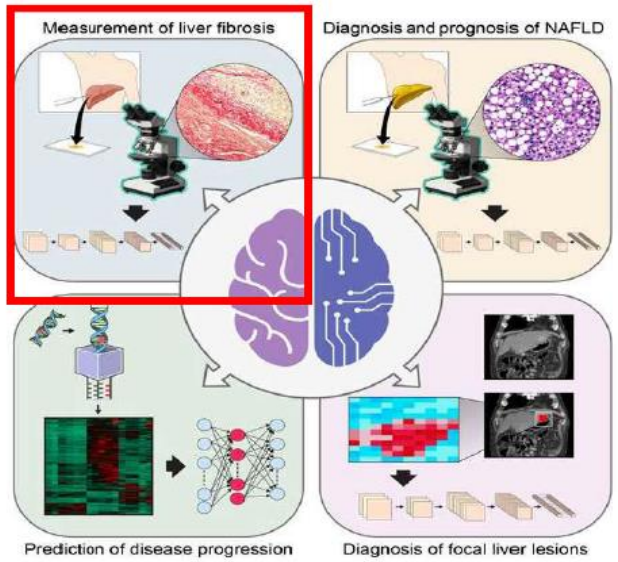

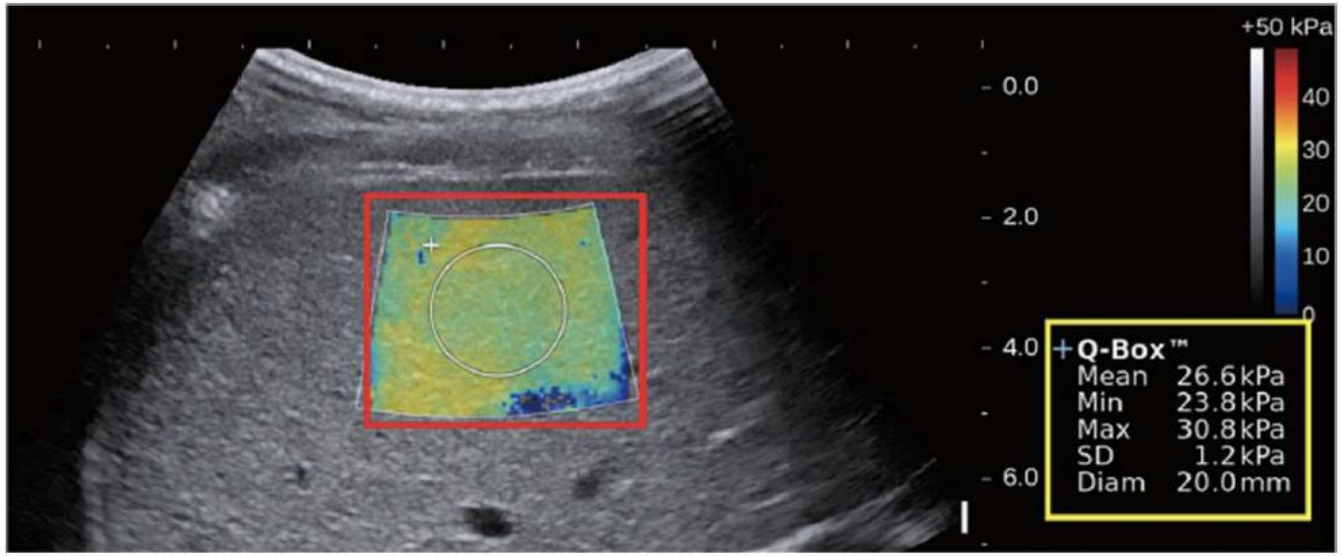

ORIGINAL RESEARCH · GASTROINTESTINAL IMAGING

Radiology

Noninvasive Diagnosis of Nonalcoholic Fatty Liver Disease and Quantification of Liver Fat with Radiofrequency Ultrasound Data Using One-dimensional Convolutional Neural Networks

Aiguo Han, PhD • Michal Byra, PhD • Elhamy Heba, MD[1] • Michael P. Andre, PhD • John W. Erdman, Jr, PhD • Rohit Loomba, MD, MHSc • Claude B. Sirlin, MD • William D. O'Brien, Jr, PhD

Performance Metrics	Input: RF without TGC
Sensitivity	97 (90, 100) [68/70]
Specificity	94 (79, 99) [30/32]
PPV	97 (90, 99) [68/70]
NPV	94 (79, 98) [30/32]
Accuracy	96 (90, 99) [98/102]

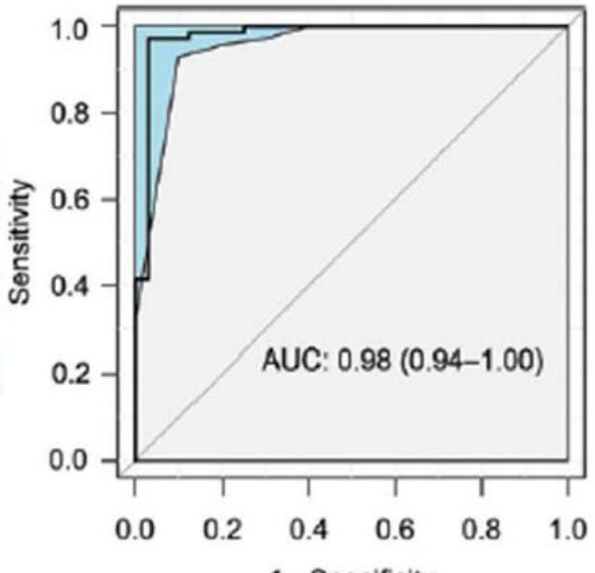

- Raw radiofrequency ultrasound contain more information than do gray-scale B-mode images because information is lost or altered when B-mode images are generated from the raw data
- A one-dimensional CNNs for NAFLD diagnosis and liver fat quantification was developed, using MRI PDFF as the reference standard.
- 204 partecipants were prospectively enrolled, equally divided into training (n = 102) and test (n = 102) groups by using stratified randomization NAFLD was defined as MRI PDFF of 5% or greater.
- Two one-dimensional CNN algorithms were developed: a binary classifier and a fat fraction estimator. For each RF signal input, the classifier output an NAFLD classification score between 0 and 1, and the fat fraction estimator output the predicted fat fraction as a percentage.

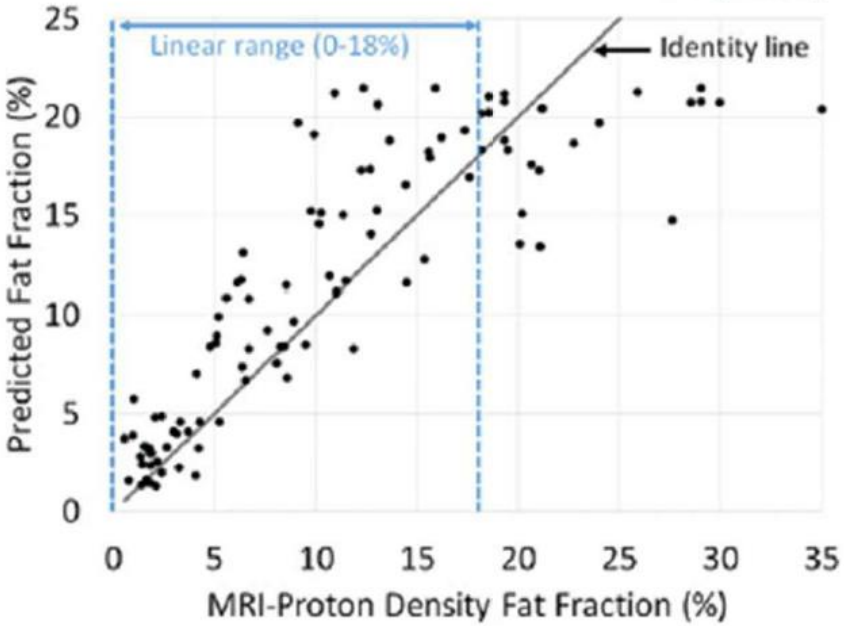

BJR

Received:
17 May 2022 | Re
11

Cite this article as:
Wei H, Shao Z, Fu
and grading inflam

Figure 3. ROC curves of the models for predicting the stage of liver fibrosis and the grade of inflammatory activity

(a), (b) ROC curves for models built based on radiomics features of T_1W, T_2WFS, and T_1W&T_2WFS images for discriminating fibrosis stage $F \geq 1$and $F \geq 2$; (c), (d) ROC curves for models built based on radiomics features of T_1W, T_2WFS, and T_1W&T_2WFS images for discriminating inflammatory activity grade $A \geq 1$and $A \geq 2$. ROC, receiver operating characteristic.

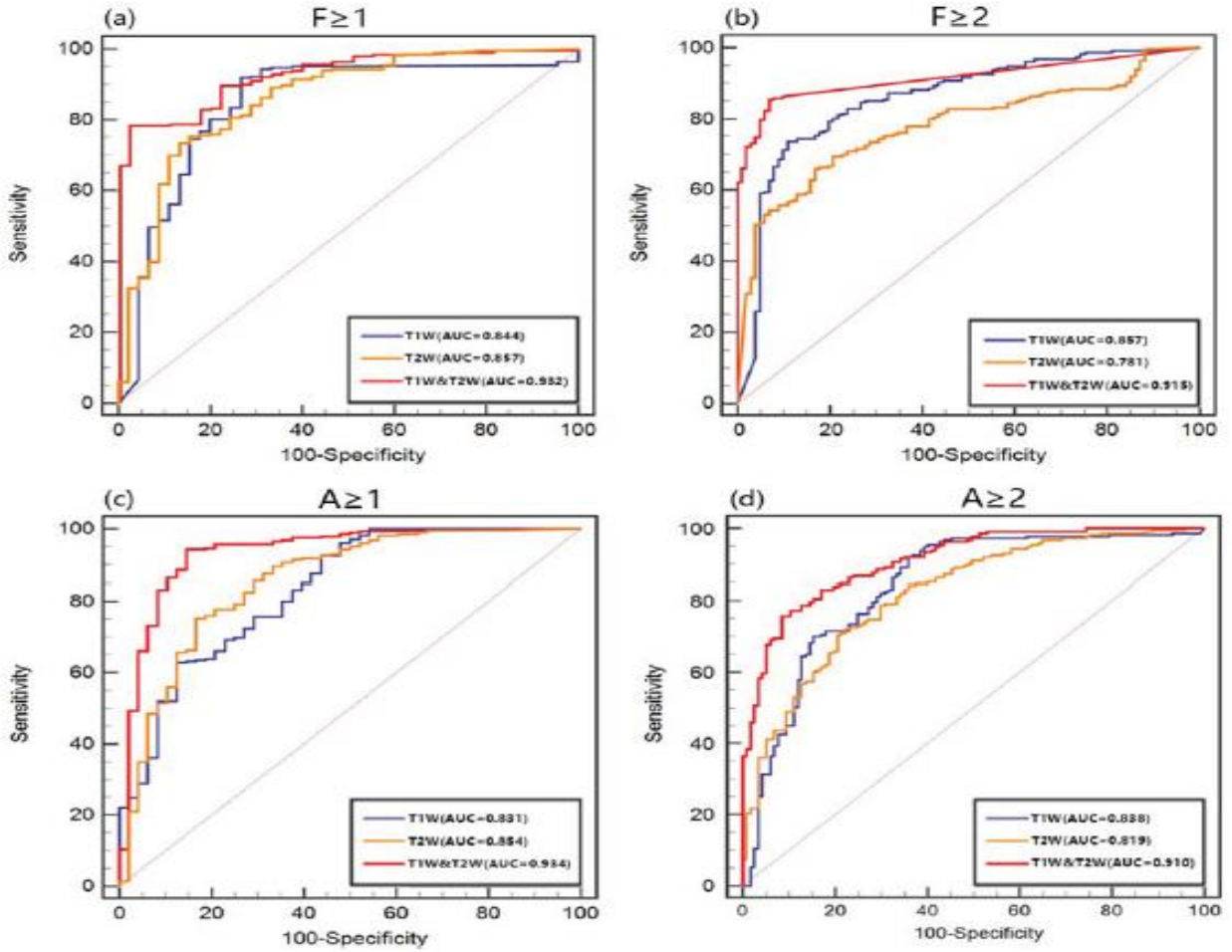

ish Institute of Radiology
org/10.1259/bjr.20220512

g staging liver fibrosis

Table 2. Magnetic resonance

Magnetic resonance sequenc			Resolution ratio	
T_1W		nm	0.74 x 0.74	
T_2WFS		nm	0.74 x 0.74	

FOV, field of view; NEX, number

Methods:
ML was app
(training set
The outc

Results: The
subjects. M
prognosis.
Cluster 1 (n
Cluster 2 (n
Cluster 3 (n
Cluster 4 (n

Conclusion
prognosis a

Therapy-in

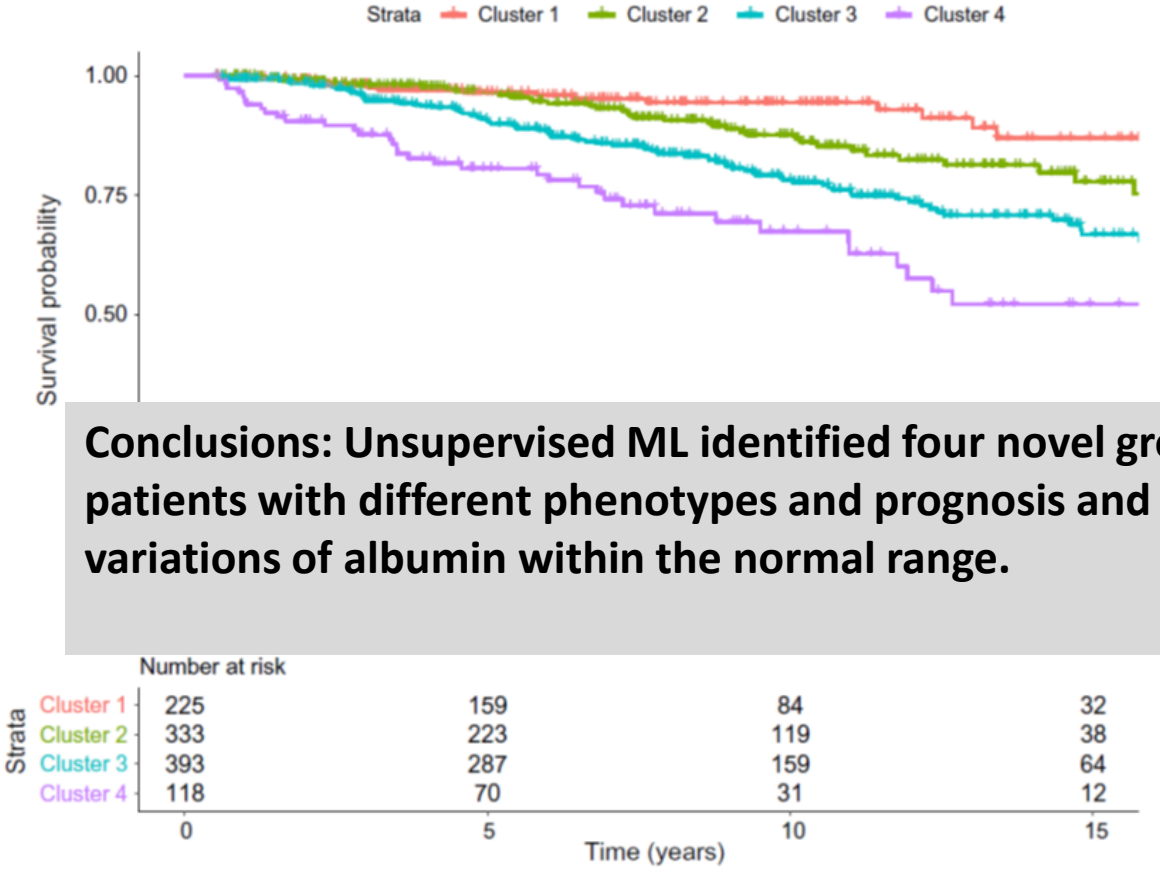

FIGURE 3 Transplant-free survival of patients by cluster membership in the validation set. The survival function within each cluster of patients with primary biliary cholangitis in the validation set was estimated using the Kaplan–Meier method and compared using the log-rank test

Conclusions: Unsupervised ML identified four novel groups of PBC patients with different phenotypes and prognosis and highlighted subtle variations of albumin within the normal range.

Patient ID	Serum bilirubin at diagnosis (x ULN)	Serum albumin at diagnosis (x LLN)	Serum ALP at diagnosis (x ULN)
DD	1.00	1.11	7.45
LF	0.73	1.23	1.09
PV	1.32	1.11	2.19

Abbreviations: LLN, lower limit of normal; ULN, upper limit of normal.

TABLE 3 Features at diagnosis of three newly diagnosed patients with primary biliary cholangitis